Adsorption and reaction of $Rh(CO)_2(acac)$ on $Al_2O_3/Ni_3Al(111)$

Y. Lei,[a] A. Uhl,[b] C. Becker,[c] K. Wandelt,[d] B. C. Gates,[e] R. Meyer*[a] and M. Trenary[b]

Received 22nd July 2009, Accepted 9th November 2009
First published as an Advance Article on the web 9th December 2009
DOI: 10.1039/b914323h

The $Al_2O_3/Ni_3Al(111)$ surface has been used as a template for the nucleation and growth of rhodium clusters using an organometallic precursor: $Rh(CO)_2(acac)$. When $Rh(CO)_2(acac)$ is deposited on the $Al_2O_3/Ni_3Al(111)$ surface, the molecule is observed to bind preferentially to specific sites associated with the film superstructure (known as the dot structure) and appears to be stable at temperatures up to 473 K at which point some sintering and aggregation processes begin. Annealing the sample to 673 K results in further sintering of the metal deposits as well as an apparent loss in the coverage of rhodium species possibly due to a combination of desorption and deligation. After annealing to 873 K the coverage of rhodium species decreases by about 50% with respect to the initial deposited coverage. Our results suggest that using an organometallic precursor rather than metal atoms to form deposited metal particles on oxide substrates may result in increased resistance to sintering processes.

Introduction

Interest in supported metal clusters has surged as researchers have demonstrated exciting, unique catalytic activity of clusters with 10 atoms or less for a number of potentially interesting reactions.[1] These clusters have been prepared by evaporative deposition of metals and "soft landing" of size selected clusters or alternatively by adsorption of molecular clusters such as metal carbonyls or synthesis of molecular clusters from organometallic precursors on support surfaces. Since evaporative deposition of such clusters is not a scalable synthesis route, much of this work has been done with ligated metal clusters (typically metal carbonyls) such as $Ru_3(CO)_{12}$,[2] $Rh_6(CO)_{16}$,[3] $H_3Re_3(CO)_{12}$,[4] and $Ir_4(CO)_{12}$.[5] Under mild conditions, these metal carbonyl precursors can sometimes be decarbonylated by heating in helium (or H_2), and intact metal cluster catalysts can be created, but these treatments may also result in cluster fragmentation or aggregation.[6] Although not every metal at every cluster size is possible, this method for synthesizing clusters allows for precise size control and it lends itself to high-surface-area supports such as those used in practical catalysts. Gates *et al.* have shown in a number of instances that the catalytic properties of supported metal clusters created from organometallic precursors are dependent on the cluster size and interaction with the support,[6–10] but the potential for such cluster catalysts is still only beginning to be realized and much remains to be understood about them.

In a similar fashion, mononuclear metal complexes can be used to generate larger metal complexes *in situ*. Although yields are not 100%, the use of mononuclear precursors can prove advantageous when dealing with zeolites or other supports with small pore sizes that do not allow entry of metal clusters as large as, for example, $Ir_4(CO)_{12}$.[11] For example, $HIr_4(CO)_{11}^-$ can be synthesized on MgO from $Ir(CO)_2(acac)$ in the presence of CO.[12] In some cases, the use of the mononuclear species appears necessary to produce deligated metal clusters. In their investigation of the adsorption of $Rh(CO)_2(acac)$ and $Rh_6(CO)_{16}$ on a Degussa P25 titania powder support (a high-area mixture of anatase and rutile), Goellner and Gates found that when $Rh_6(CO)_{16}$ was deposited directly on the titania surface, aggregates were formed, and decarbonylation by treatment in hydrogen resulted in destruction of the Rh_6 frame along with rhodium sintering.[13] In contrast, adsorption of $Rh(CO)_2(acac)$ followed by treatment in CO at 373 K resulted in the formation of site-isolated $Rh_6(CO)_{16}$ in high yield, which could then be treated in helium (or hydrogen) at temperatures of up to 573 K for apparently complete removal of the CO ligands, leaving the Rh_6 frame intact as well as could be determined from EXAFS (extended X-ray absorption fine structure) spectroscopy measurements of Rh–Rh coordination numbers and bond distances.

Although EXAFS spectroscopy, high-resolution TEM (transmission electron microscopy), and other techniques have been used to provide some understanding of the chemistry of cluster synthesis on supports, much has only been inferred, and many questions remain, such as the identity of the exact placement of the precursors on the support surfaces and how defect sites and nonuniformity of the high-area powder supports affect the cluster synthesis process and ultimately the catalyst performance. To gain insight into the molecular level cluster formation processes, it would be advantageous to image the surface species. Thus, we were motivated to investigate the chemistry of cluster formation on a well-characterized planar

[a] *University of Illinois at Chicago, Department of Chemical Engineering, Chicago, IL 60607, USA*
[b] *University of Illinois at Chicago, Department of Chemistry, Chicago, IL 60607, USA*
[c] *CINaM – CNRS – UPR 3118, associated to Université de la Méditerranée and Université Paul Cézanne, Campus de Luminy – Case 913, 13288 Marseille Cedex 09, France*
[d] *Univeristät Bonn, Institut für Physikalische und Theoretische Chemie, Wegelerstr. 12, 53115 Bonn, Germany*
[e] *University of California at Davis, Department of Chemical Engineering and Materials Science, Davis, CA 95616, USA*

substrate using a combination of imaging and spectroscopic methods. Building upon the work of Goellner and Gates, illustrating formation of Rh_6 from $Rh(CO)_2(acac)$, we now adopt a surface science approach to characterization of cluster synthesis.

Early work in this direction was carried out in the collaboration of Goodman and Gates *et al.*[14,15] They adsorbed rhenium carbonyl species, $HRe(CO)_5$ and $Re_2(CO)_{10}$, on MgO thin films grown on Mo(110). However, these combined temperature programmed desorption–reflection absorption infrared spectroscopy (TPD/RAIRS) experiments failed to provide precise structural relationships between the rhenium subcarbonyls and the thin film support surface, and cluster formation was not characterized. Supported Rh organometallic precursors have also been studied previously on single crystal $TiO_2(110)$ surfaces,[16–22] primarily in the group of Hayden. One of the observations of Hayden's work is that the identity of the rhodium precursor ($[Rh(CO)_2Cl]_2$ *vs.* $Rh(acac)(CO)_2$) led to very different catalytic selectivities of the resultant species in CO hydrogenation reactions, providing clear evidence that the surface chemistry of the organometallic complex plays an important role in determining the reactivity of the formed nanoclusters.[23,24] Using RAIRS and X-ray photoelectron spectroscopy (XPS), Hayden and co-workers established that the support-anchored rhodium gem dicarbonyl species formed an intermediate upon exposure to hydrogen at room temperature, which they suggested is likely to be HRhCO.[21] The authors showed that this monocarbonyl intermediate could be reconverted to $Rh(CO)_2$ upon exposure to CO or could be completely reduced to rhodium metal particles upon heating to 475 K (the reduction is accompanied by aggregation of the metal).

One of the key questions that arose in the prior work of Gates and Goodman *et al.*[14,15] is the structural relationship between the precursor and the substrate. Recently, Goodman and Adams *et al.* have examined the behavior of $Ru_3(CO)_9(Sn(C_6H_5)_2)_3$ adsorbed on a SiO_2 thin film grown on Mo(112).[25] Using STM, Adams and Goodman *et al.* found that the intact metal framework of clusters could be imaged after deligation by heating to 450 K. One interesting aspect of this work is that the clusters were deposited *ex situ* by applying droplets of a toluene solution containing the Ru_3Sn_3 organometallic to the SiO_2 coated Mo(112) single crystal. After rapid evaporation of the organic solvent, the crystal was moved back into the vacuum chamber for characterization. STM images also appear to show a distinct relationship between the deligated metal cluster structure and the underlying SiO_2 substrate as the Ru_3 center sits preferentially atop SiO_4 tetrahedra.

In order to establish precise relationships between the adsorption site and the supported organometallic species, we have used a surface with a precisely defined atomic structure: an Al_2O_3 thin film grown from preferential oxidation of $Ni_3Al(111)$. The $Al_2O_3/Ni_3Al(111)$ film, developed by Becker and co-workers,[26,27] possesses regular long-range order and lacks phase boundaries. Interestingly, when metal atoms are deposited upon these films, particle nucleation may occur at a regular spacing of 4.16 nm. This observation has been attributed to the corrugation in the potential energy surface created by commensuration of the alumina film with the underlying metal substrate and the distortion of the corundum structure.[27,28] Becker and co-workers have recently used this surface to achieve a nearly monodisperse distribution of small Pd clusters.[29] The "defects" have been shown to strongly bind Mn, V, Fe, and Pd, leading to patterned surfaces, although Au and Ag particles have been observed to diffuse readily on this surface at room temperature.[30–33] Although it might be expected that Rh atoms should behave similarly to Pd atoms, the roles of the ligands on our organometallic precursors may lead to entirely different behavior. To test the chemistry involving the organometallic rhodium species we have imaged $Rh(CO)_2(acac)$ deposits on $Al_2O_3/Ni_3Al(111)$ at room temperature after annealing to a wide range of temperatures using scanning tunneling microscopy (STM) in an effort to understand how these species nucleate, deligate and agglomerate on the support surface.

Experimental

All the deposition experiments were done at the University of Illinois at Chicago in ultra-high vacuum with a variable-temperature scanning tunneling microscope (VT-SPM, Omicron) system consisting of a STM chamber and a separate preparation chamber. The preparation chamber is equipped with low energy electron diffraction optics (SPEC3), a metal evaporation source (EFM3), and a home-made organic compound evaporator. The base pressure was $\sim 1 \times 10^{-10}$ mbar during the STM experiments. The $Ni_3Al(111)$ single crystal (MaTeck, Jülich, Germany) used in the sequential $Rh(CO)_2(acac)$ deposition experiments was polished on one side and mounted on a standard tantalum sample plate from Omicron with a 8 mm diameter hole cut in the back to facilitate electron bombardment heating. The temperature was previously calibrated with a type K thermocouple welded to the edge of the $Ni_3Al(111)$ crystal. At high temperatures (above 900 K), the temperature of the crystal could be precisely monitored by a pyrometer (Omega) using an emissivity of 0.48 for the Ni_3Al crystal (the emissivity was determined during the thermocouple calibration).[34]

Thin films of Al_2O_3 supported on a $Ni_3Al(111)$ single crystal were grown using the recipe developed by Becker and co-workers.[27,29,35–37] The clean and ordered $Ni_3Al(111)$ surface was prepared by repeated cycles of Ar^+ ion sputtering (2.5 keV, 10 μA cm^{-2}) at a sample temperature of 600 K for about 15 min, with subsequent annealing at 1150 K for 10 min and 1000 K for 10 min, respectively. Alumina thin films were grown by oxidation of the clean $Ni_3Al(111)$ surface at 1000 K at an oxygen partial pressure of 4×10^{-8} mbar. The Ni_3Al surface was exposed to 40 L (1 L = 10^{-6} Torr s) of oxygen, followed by annealing at 1050 K for 5 min. This cycle was normally repeated twice to obtain a closed alumina film with a high degree of long-range order. LEED patterns characterizing the film were compared with those previously reported by Degen *et al.*[27]

Exposure of the sample surface to $Rh(CO)_2(acac)$, rhodium(I) dicarbonylacetylacetonate (Strem, 99%), was done in the preparation chamber by means of physical vapor deposition (PVD) using a home-made organic compound

doser. $Rh(CO)_2(acac)$ was stored in a glass tube under vacuum and was heated with electrical heating tape. The temperature was measured with a type K thermocouple attached to the tube's wall. The solid $Rh(CO)_2(acac)$ was typically heated to between 330 and 350 K to achieve a substantial vapor pressure (we did not measure this directly). The $Rh(CO)_2(acac)$ vapor was delivered to the preparation chamber *via* a leak valve, and a stainless steel tube with 1 cm inner diameter was employed to direct the organic compound to the target surface. During the dosing, the distance between the opening of the stainless steel tube and the sample surface was about 1 mm in order to increase the dosing efficiency with minimum background exposure. All deposition experiments were performed with the $Al_2O_3/Ni_3Al(111)$ crystal at room temperature.

Determination of the coverage of deposited rhodium species is complicated by the fact that some of the organometallic species seem to deposit intact on the surface as isolated species while some material aggregates rapidly even at room temperature. Therefore, the absolute coverage is estimated in the following way. As will be discussed below in more detail, we will assume that the clusters present after annealing of the sample to 1073 K must be pure rhodium. On the basis of this assumption, we can calculate the surface coverage of rhodium. By further assuming that the clusters are hemispherical in shape and measuring cluster heights, radii and surface densities from the STM images, an estimate of the total amount of rhodium can be made based on the packing of Rh atoms (7.26×10^{22} atoms per cm^3 or 73 atoms per nm^3).

STM images were collected with electrochemically etched commercial Pt–Ir tips (Agilent Technologies) with sample biases of 0.7–3.2 V and a constant tunneling current of 0.1 nA. All images were generated at room temperature. Images of the rhodium species on the $Al_2O_3/Ni_3Al(111)$ surface were generally acquired $\sim$1.5 h after annealing so that the sample had returned to room temperature. It should be noted that for the sub-monolayer exposure of the rhodium dicarbonylacetylacetonate deposited at room temperature, it could take up to several hours to re-condition the STM tip by applying pulses of up to 10 V.

Results and discussion

LEED pattern of clean $Ni_3Al(111)$ crystal and $Al_2O_3/Ni_3Al(111)$

The clean $Ni_3Al(111)$ surface and Al_2O_3 film were characterized by LEED (low energy electron diffraction). The LEED pattern of the clean $Ni_3Al(111)$ surface is shown in Fig. 1(a). A 2×2 superstructure can be observed from the clean crystal LEED pattern. As shown in Fig. 1(b), exposing the $Ni_3Al(111)$ surface to 40 L of oxygen at 1000 K led to the appearance of a new set of spots attributed to an oxygen-induced structure, indicating the formation of a thin Al_2O_3 film on the $Ni_3Al(111)$ surface. These results are in good agreement with previous observations of Becker *et al.*[27,35]

STM

A smooth and continuous Al_2O_3 thin film has been observed by STM as shown in Fig. 2(a–c). Different superstructures could be observed by tuning the bias voltage over the range from 0.7 to 3.2 V. As shown in Fig. 2(a), when a bias voltage of 0.7 V was applied, a pattern of hexagonal structures with minimal corrugation emerged. A more detailed image of the superstructure is shown in Fig. 3(a). When the bias voltage was elevated, the centers of these hexagonal structures became prominent so that the "dot structure" with a periodicity of 4.1 nm was revealed, as shown in Fig. 2(b). The white open circles shown in Fig. 3(a) correspond to the bright dots in Fig. 2(b). Further increasing the bias voltage to 3.2 V revealed the pattern of the "network structure" in Fig. 2(c) with a periodicity of 2.4 nm. Kresse and co-workers have determined that the dot structure is defined by "holes" in the film where surface oxygen is missing and that the network structure is defined by a combination of these holes with threefold symmetry sites formed by replacement of the hexagonal corundum structure with three pentagons and an Al_3 triangle in the interface layer between the Al_2O_3 film and the underlying $Ni_3Al(111)$ substrate.[38] The dark spots in the pattern of the "network structure" in Fig. 2(c) correspond to both the blue and white open circles in Fig. 3(a). The dot superstructure has been observed to be the preferential nucleation site for adsorption of Pd, whereas other metals such as Fe and V have been observed to nucleate over the network structure.[29,30,32,33]

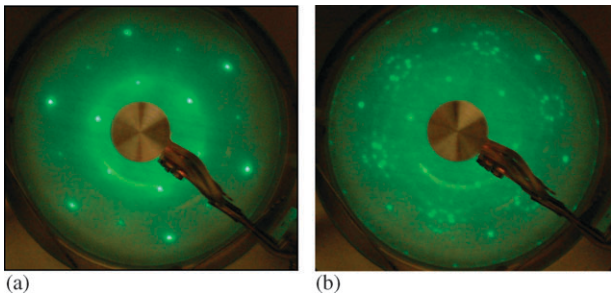

Fig. 1 LEED pattern of (a) the clean Ni_3Al (111) surface, (b) after 40 L O_2 exposure at 1000 K, the LEED images were taken at 93 eV primary energy.

Using the calibration method we describe in the Experimental section, 0.06 ML of rhodium in the form of $Rh(CO)_2(acac)$ was dosed onto the $Al_2O_3/Ni_3Al(111)$ substrate. At room temperature, $Rh(CO)_2(acac)$ can be observed to homogenously nucleate on the dot structure sites as single molecules with a height of $\sim$0.15 nm and a mean distance of 4.1 ± 0.1 nm, as shown in Fig. 3(b). This distance is similar to the distance between the white open circles shown in Fig. 3(a). The height of the brighter spot at the center of Fig. 3(b) is about 0.3 nm, possibly corresponding to a dimer of the rhodium species.

Care must be taken when imaging clusters on the thin oxide film because the characteristic superstructure of the film itself in the STM images is strongly bias-dependent. Hence, proper imaging conditions for probing the surface had to be established. From Fig. 2(a), it has been established that the dot structure of the film vanishes as the bias is decreased to 0.7 V such that the film possesses minimal corrugation on the order of 0.01 nm (although a hexagonal pattern is faintly visible). Therefore, by imaging our precursor at low bias, we can accurately determine its height.

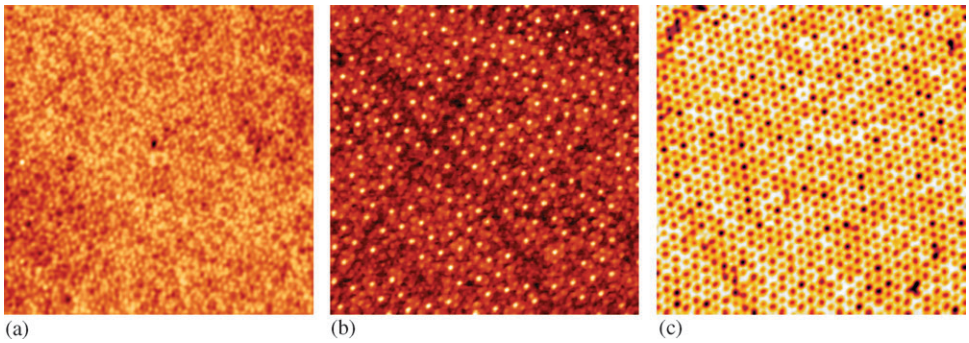

Fig. 2 STM images of the clean $Al_2O_3/Ni_3Al(111)$ surface with bias voltages of: (a) 0.7 V, (b) 2.3 V and (c) 3.2 V. The tunneling current was 0.1 nA. Each image is 70 nm × 70 nm.

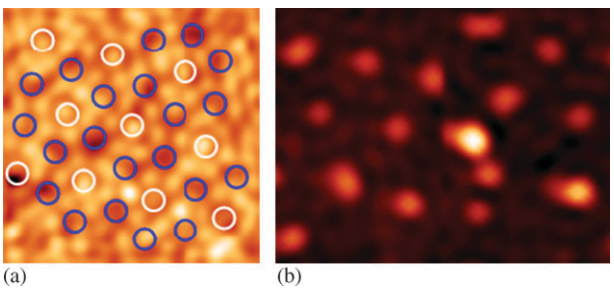

Fig. 3 STM images of (a) clean $Al_2O_3/Ni_3Al(111)$ surface, 15 nm × 15 nm, (b) $Rh(CO)_2(acac)/Al_2O_3/Ni_3Al(111)$ as-deposited at room temperature, 15 nm × 20 nm. Bias voltage: 0.7 V. Tunneling current 0.1 nA. The circles are meant to guide the eye to the dot (white circles only) and network (white + blue circles) structures of the Al_2O_3 film.

The bias dependence of features of the $Rh(CO)_2(acac)$ that was deposited at room temperature and annealed at 523 K is shown in Fig. 4. As shown in Fig. 4(a), when a bias voltage of $V_b = 0.7$ V was used, clusters could be clearly imaged along with the underlying smooth and flat periodic hexagonal superstructure of the Al_2O_3 film. In this case only the clusters were imaged as protrusions. Fig. 4(b) shows the resulting STM image for a bias voltage of $V_b = 2.3$ V. Under these imaging conditions both the clusters and the 'dot structure' appeared as protrusions, while the periodic pattern of the film was also revealed (in fact the structure of the film appears as a hybrid between the dot structure and the network structure in this case where the dots appear as protrusions but the threefold symmetry sites appear as holes). The blue arrows in the two images mark the same cluster. Comparing the images, we can observe that the large protrusions present in Fig. 4(a) clearly represent clusters. Therefore, in order to unambiguously identify clusters, a low bias ($V_b = 0.7$ V) had to be used such that only clusters were visible as protrusions. However, scanning at $V_b = 2.3$ V helped us establish relationships between nucleation of the precursor and the geometry of the underlying substrate.

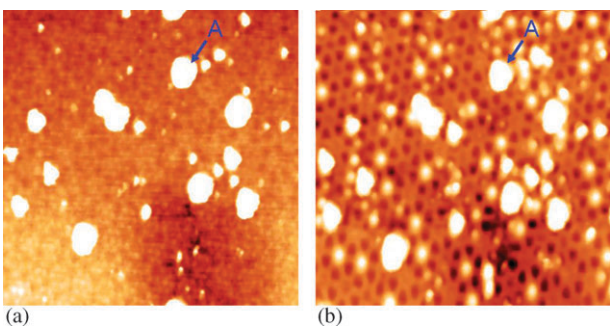

Fig. 4 STM images of rhodium species deposited at room temperature and then annealed at 523 K with bias voltage (a) $V_b = 0.7$ V, (b) $V_b = 2.3$ V. Tunneling current was 0.1 nA for each image. Each image is 55 nm × 55 nm. The blue arrows show the same particle in each image.

Fig. 5 reveals the growth process of rhodium clusters on the surface as a function of annealing temperature. We began by depositing $Rh(CO)_2(acac)$ on $Al_2O_3/Ni_3Al(111)$ at room temperature as depicted in Fig. 5(a). The adsorbed $Rh(CO)_2(acac)$ monomer primarily nucleated on the dot structure sites and had a height of ~0.15 nm. The "molecular" species (we cannot be absolutely certain that the molecule is

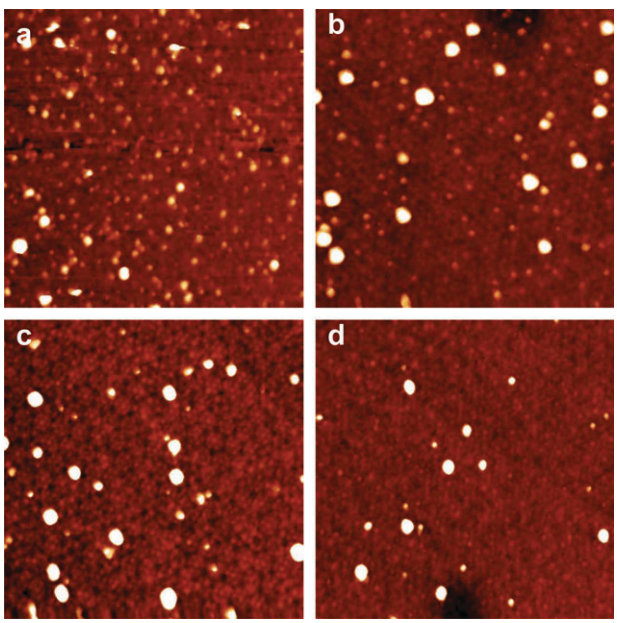

Fig. 5 STM images of rhodium species deposited as $Rh(CO)_2(acac)$ at room temperature (a) no anneal, and after annealing at the following temperatures for 5 min: (b) 473 K, (c) 673 K, (d) 873 K. Each image is 70 nm × 70 nm. Each image was taken at $V_b = 0.7$ V and 0.1 nA.

completely unreactive on the surface, although this seems to be a reasonable assumption) were found to be stable on the Al_2O_3 dot structure from room temperature up to 423 K. Neither the size distribution nor the surface coverage of the molecular species significantly changed in this temperature range. However, it appears that some of these organometallic species had already agglomerated at room temperature as features on the surface were also present with a height up to ~1 nm on the surface. As we have mentioned in the Experimental section, we ultimately estimate the coverage of rhodium based upon the assumption that the clusters are pure rhodium after annealing to 1073 K. There are two important implications of this assumption. First, the large clusters present at room temperature are not likely to have been aggregated as intact precursor molecules but must already have been partially deligated. Second, these larger features actually make up the majority of the total mass (volume) of the deposited species. So although the precursor has been shown to nucleate on the dot structure, large amounts of material were not nucleated at the high-symmetry sites on the surface but rather easily diffused and aggregated even at room temperature.

However, after annealing of the sample to 473 K, the number of large agglomerates on the Al_2O_3 surface increased with the decrease of surface particle density shown in Fig. 5(b), although the coverage of rhodium species on the surface remained constant. The number of molecular species on the surface appears to have decreased. Fig. 5(c) shows that further annealing the sample to 673 K resulted in a further decrease in the number of molecular species. At 673 K, the total coverage of rhodium species also started to decrease. Of course, without the use of other techniques, we cannot determine when the rhodium clusters begin to deligate, but we may speculate that the decrease in coverage could be related to removal of CO or other species from the rhodium nucleus. By 673 K, one must assume that all of the CO has left the surface or has dissociated into O atoms and C atoms on the surface of the rhodium particles (CO dissociation is possible on small rhodium particles[39]). Similarly, the acetylacetonate ligand has likely decomposed or desorbed at this point. Therefore, our rhodium particles may actually contain significant amounts of both carbon and oxygen.

After annealing the sample to 873 K, the coverage of rhodium particles dropped to less than 50% of the coverage at room temperature and the predominant surface species were large aggregates of rhodium. Freund and co-workers found, by using PVD to deposit rhodium nanoparticles on an Al_2O_3/NiAl(110) surface, that after annealing at 870 K nearly all the rhodium particles had disappeared from the surface, probably due to migration of rhodium atoms into the film.[40] Density functional theory calculations suggest that palladium atom migration into "holes" in the $Ni_3Al(111)$ film should be facile, and it seems likely that rhodium would behave in a similar manner.[38] However, our results suggest that when $Rh(CO)_2$(acac) is deposited on $Ni_3Al(111)$, rhodium diffusion into the $Al_2O_3/Ni_3Al(111)$ surface is inhibited, possibly due to the presence of residual carbon from either the carbonyl or acac ligands, since 50% or more of the initially deposited material remains on the surface. Moreover, when $Rh/Al_2O_3/Ni_3Al(111)$ was further annealed at 1050 K for 5 minutes, rhodium particles could still be easily observed on the surface (shown in Fig. 8(a)).

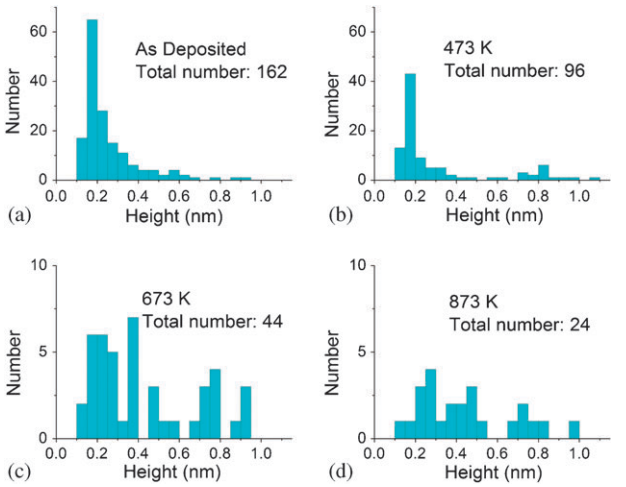

Fig. 6 Height distribution of rhodium species formed from $Rh(CO)_2$(acac) deposited at room temperature (a) no anneal, and after annealing at the following temperatures for 5 min: (b) 473 K, (c) 673 K, (d) 873 K.

Fig. 6(a–d) show the height distribution of rhodium particles annealed at various temperatures as determined by STM imaging. Fig. 6(a–d) show particle size distributions from single representative images at each temperature. A narrow height distribution was obtained in the as-prepared sample after deposition of the $Rh(CO)_2$(acac) precursor at room temperature, as shown in Fig. 6(a). Most of the particles are inferred to be monomers of $Rh(CO)_2$(acac) with heights of between 0.15 and 0.2 nm with a few large particles on the surface. After annealing of the sample to 473 K, about half of the monomers sintered into large aggregates. The surface species exhibited a bimodal height distribution, with small clusters of approximately 0.15 nm (again presumed to be $Rh(CO)_2$(acac) molecules) and large particles of approximately 0.8 nm (Fig. 6(b)). The height of a rhodium layer was about 0.23 nm, suggesting formation of rhodium particles with a thickness of 3–4 atomic layers. After annealing to 673 K, the surface species still exhibited a bimodal height distribution. However, the center of the height distribution for small particles shifted towards large values, from ~0.15 nm to about 0.25 nm, due to the significant decrease in the number of $Rh(CO)_2$(acac) monomers. A second group of clusters was characterized by an average height of approximately 0.8 nm. After annealing to 873 K, the center of the height distribution for small clusters further shifted towards larger values (~0.3 nm) with some aggregates showing a height of more than 1 nm. At this temperature, all the monomeric rhodium species with heights of ~0.15 nm were eliminated.

Although the apparent radii obtained from STM images are known to be overestimated because of tip convolution effects,[41] the changes in measured radius follow the same trend as changes in actual particle radius. The radius distributions can also supplement our understanding of how the cluster shapes develop during the whole annealing process. Fig. 7(a–d) show the distributions of radii of rhodium particles in our samples annealed at various temperatures. Similar to

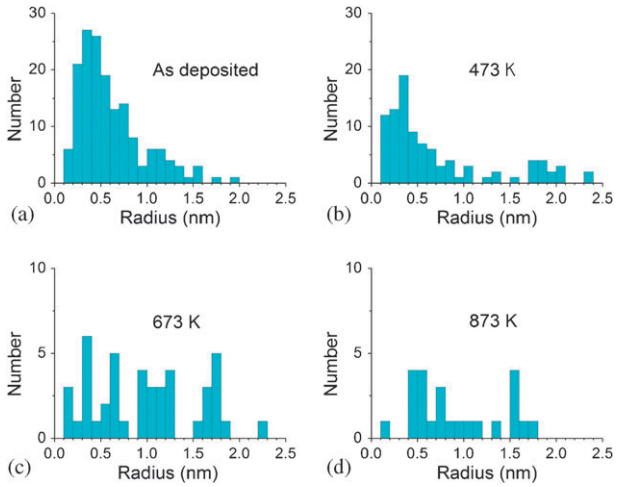

Fig. 7 Size distribution of rhodium species deposited as $Rh(CO)_2(acac)$ at room temperature (a) no anneal, and after annealing at the following temperatures for 5 min: (b) 473 K, (c) 673 K, (d) 873 K.

the height distribution, there was a single center at ~0.4 nm in the distribution of radii for the image characterizing the as-prepared sample (Fig. 7(a)). The distribution of radii is broader due to the tip convolution effects.

After annealing to 473 K, a bimodal size distribution appeared once again, with an average radius of ~0.4 nm for small clusters and a second grouping with an average radius of ~1.9 nm for larger particles. After annealing to 673 K, the radial distribution center for the larger particles shifted to slightly smaller values (~1.7 nm).

Finally, annealing to 873 K resulted in a further decrease of the average radius of the larger particles to ~1.5 nm, possibly as a consequence of further deligation. Combining the results characterizing the particle radii and height distributions, we conclude that clusters with a narrow size distribution can be obtained initially using $Rh(CO)_2(acac)$ as a precursor. After annealing of the alumina thin film supported rhodium samples to 473 K, a bimodal size distribution of supported clusters emerged. Annealing the sample further to 673 K and then 873 K led to a decrease in the surface particle density as molecular (or monomer) rhodium species underwent sintering, but the larger aggregates actually showed some decrease in diameter.

Fig. 8(a) shows the three dimensional growth of rhodium particles on the $Al_2O_3/Ni_3Al(111)$ surface after annealing of the sample to 1050 K. Only large rhodium islands could be found on the surface after annealing at this temperature. The size of the rhodium particles could be up to ~0.7 nm in height and ~3 nm in radius. A profile of one of the rhodium islands is shown in Fig. 8(b). The shape of the island was no longer hemispherical. The profile appears to indicate that a three-layer rhodium particle had formed with each layer having a thickness of approximately 0.21 nm. In a previous study, Bäumer and Freund observed 3D rhodium particles on the $Al_2O_3/NiAl(110)$ surface similar in shape to those of Fig. 8 when 2 ML of rhodium was deposited at room temperature using a metal evaporator.[42] Our results show that, with a sub-monolayer deposition of $Rh(CO)_2(acac)$, only at a temperature as high as 1050 K will rhodium aggregates form that resemble 3D metallic islands.

Conclusion

When $Rh(CO)_2(acac)$ is deposited on the $Al_2O_3/Ni_3Al(111)$ surface, well-ordered rhodium clusters with a narrow size distribution can be fabricated on the surface. The rhodium organometallic precursor nucleates at specific sites associated with the film superstructure and appears to be stable at temperatures up to 473 K. At 473 K, visible aggregation of rhodium begins on the surface and particles with a bimodal size distribution are formed. Annealing the sample to 673 K results in a decrease in the apparent surface coverage of rhodium possibly due to a combination of desorption and deligation. Monomers of the rhodium precursor disappear completely after annealing to 873 K and the surface coverage of rhodium decreases by about 50% with respect to the initial

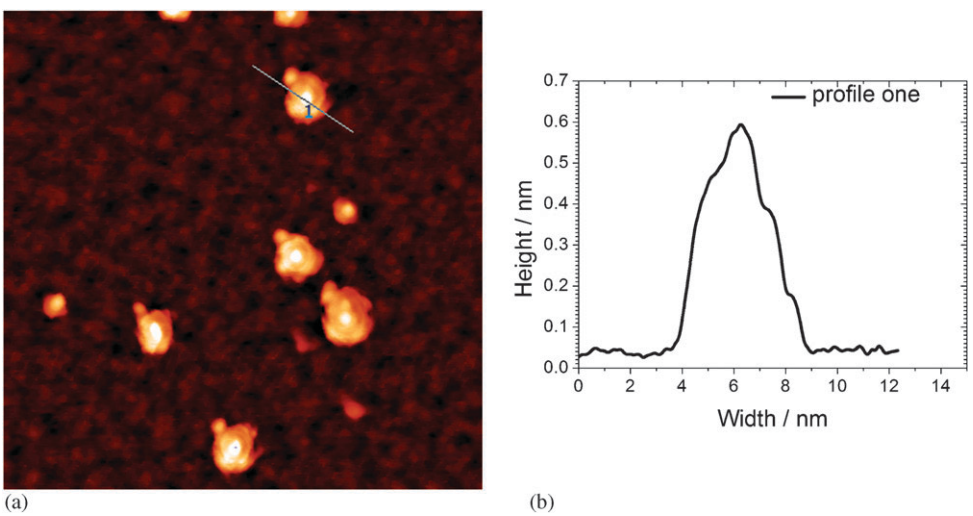

Fig. 8 (a) STM image of rhodium species deposited on $Al_2O_3/Ni_3Al(111)$ at room temperature followed by annealing at 1050 K, (b) line profile of chosen island. Image (a) is 50 nm × 50 nm recorded with V_b = 0.7 V and I_T = 0.1 nA.

coverage of the deposited species. However, at 1050 K, large 3D rhodium islands with clear layers are observed. Although our results are merely an initial step in the investigation of sintering and deligation of these species on oxide surfaces, they suggest that distinct links between oxide surface properties and the aggregation of metal clusters can be made.

Acknowledgements

A.U. and M.T. acknowledge support by the National Science Foundation under grant CHE-0714562. Y.L. and R.M. acknowledge support by the Petroleum Research Fund grant # 46131-G5. BCG acknowledges support by the Department of Energy, Office of Energy Research, Basic Energy Sciences grant # DE-FG02-04ER15600.

References

1 U. Heiz and E. L. Bullock, *J. Mater. Chem.*, 2004, **14**, 564–577.
2 J. Robertson and G. Webb, *Proc. R. Soc. London, Ser. A*, 1974, **341**, 383.
3 J. L. Bilhou, V. Bilhou-Bougnol, W. F. Graydon, J.-M. Basset, A. K. Smith, G. M. Zanderighi and R. Ugo, *J. Organomet. Chem.*, 1978, **153**, 73–84.
4 P. S. Kirlin, F. A. De Thomas, J. W. Bailey, H. S. Gold, C. Dybowski and B. C. Gates, *J. Phys. Chem.*, 1986, **90**, 4882–4887.
5 S. D. Maloney, F. B. M. van Zon, M. J. Kelley, D. C. Koningsberger and B. C. Gates, *Catal. Lett.*, 1990, **5**, 161–168.
6 J. Guzman and B. C. Gates, *Dalton Trans.*, 2003, 3303–3318.
7 Z. Xu, F. S. Xiao, S. K. Purnell, O. Alexeev, S. Kawi, S. E. Deutsch and B. C. Gates, *Nature*, 1994, **372**, 346–348.
8 B. C. Gates, *Chem. Rev.*, 1995, **95**, 511–522.
9 A. M. Argo, J. F. Odzak and B. C. Gates, *J. Am. Chem. Soc.*, 2003, **125**, 7107–7115.
10 F. Li and B. C. Gates, *J. Phys. Chem. C*, 2007, **111**, 262–267.
11 S. Kawi and B. C. Gates, *J. Phys. Chem.*, 1995, **99**, 8824–8830.
12 S. Kawi and B. C. Gates, *Inorg. Chem.*, 1992, **31**, 2939–2947.
13 J. F. Goellner and B. C. Gates, *J. Phys. Chem. B*, 2001, **105**, 3269–3281.
14 S. K. Purnell, X. Xu, D. W. Goodman and B. C. Gates, *Langmuir*, 1994, **10**, 3057–3062.
15 S. K. Purnell, X. Xu, D. W. Goodman and B. C. Gates, *J. Phys. Chem.*, 1994, **98**, 4076–4082.
16 Y. Maeda, M. Okumura, M. Date, S. Tsubota and M. Haruta, *Surf. Sci.*, 2002, **514**, 267–272.
17 R. A. Bennett, N. D. McCavish, M. Basharn, V. R. Dhanak and M. A. Newton, *Phys. Rev. Lett.*, 2007, **98**, 056102.
18 J. Evans, B. Hayden, F. Mosselmans and A. Murray, *J. Am. Chem. Soc.*, 1992, **114**, 6912–6913.
19 J. Evans, B. Hayden, F. Mosselmans and A. Murray, *Surf. Sci.*, 1994, **301**, 61–82.
20 B. E. Hayden, A. King and M. A. Newton, *Chem. Phys. Lett.*, 1997, **269**, 485–488.
21 B. E. Hayden, A. King and M. A. Newton, *Surf. Sci.*, 1998, **397**, 306–313.
22 B. E. Hayden, A. King, M. A. Newton and N. Yoshikawa, *J. Mol. Catal. A: Chem.*, 2001, **167**, 33–46.
23 J. Evans, B. E. Hayden and M. A. Newton, *Surf. Sci.*, 2000, **462**, 169–180.
24 M. A. Newton, J. Evans and B. E. Hayden, *J. Phys. Chem. B*, 2000, **104**, 8548–8553.
25 F. Yang, E. Trufan, R. D. Adams and D. W. Goodman, *J. Phys. Chem. C*, 2008, **112**, 14233–14235.
26 C. Becker, J. Kandler, H. Raaf, R. Linke, T. Pelster, M. Drager, M. Tanemura and K. Wandelt, *J. Vac. Sci. Technol., A*, 1998, **16**, 1000–1005.
27 S. Degen, A. Krupski, M. Kraj, A. Langner, C. Becker, M. Sokolowski and K. Wandelt, *Surf. Sci.*, 2005, **576**, L57–L64.
28 T. Maroutian, S. Degen, C. Becker, K. Wandelt and R. Berndt, *Phys. Rev. B: Condens. Matter Mater. Phys.*, 2003, **68**, 155414.
29 S. Degen, C. Becker and K. Wandelt, *Faraday Discuss.*, 2004, **125**, 343–356.
30 C. Becker, K. von Bergmann, A. Rosenhahn, J. Schneider and K. Wandelt, *Surf. Sci.*, 2001, **486**, L443–L448.
31 A. Wiltner, A. Rosenhahn, J. Schneider, C. Becker, P. Pervan, M. Milun, M. Kralj and K. Wandelt, *Thin Solid Films*, 2001, **400**, 71–75.
32 C. Becker, A. Rosenhahn, A. Wiltner, K. von Bergmann, J. Schneider, P. Pervan, M. Milun, M. Kralj and K. Wandelt, *New J. Phys.*, 2002, **4**, 75–75.15.
33 A. Lehnert, A. Krupski, S. Degen, K. Franke, R. Decker, S. Rusponi, M. Kralj, C. Becker, H. Brune and K. Wandelt, *Surf. Sci.*, 2006, **600**, 1804–1808.
34 http://www.omega.com/literature/transactions/volume1/thermometers1.html.
35 A. Rosenhahn, J. Schneider, C. Becker and K. Wandelt, *J. Vac. Sci. Technol., A*, 2000, **18**, 1923–1927.
36 S. Gritschneder, C. Becker, K. Wandelt and M. Reichling, *J. Am. Chem. Soc.*, 2007, **129**, 4925–4928.
37 G. Hamm, C. Barth, C. Becker, K. Wandelt and C. R. Henry, *Phys. Rev. Lett.*, 2006, **97**, 126106.
38 M. Schmid, G. Kresse, A. Buchsbaum, E. Napetschnig, S. Gritschneder, M. Reichling and P. Varga, *Phys. Rev. Lett.*, 2007, **99**, 196104.
39 M. Frank, S. Andersson, J. Libuda, S. Stempel, A. Sandell, B. Brena, A. Giertz, P. A. Bruhwiler, M. Baumer, N. Martensson and H. J. Freund, *Chem. Phys. Lett.*, 1997, **279**, 92–99.
40 M. Heemeier, S. Stempel, S. K. Shaikhutdinov, J. Libuda, M. Bäumer, R. J. Oldman, S. D. Jackson and H. J. Freund, *Surf. Sci.*, 2003, **523**, 103–110.
41 S. Stempel, M. Baumer and H. J. Freund, *Surf. Sci.*, 1998, **402–404**, 424–427.
42 M. Bäumer and H. J. Freund, *Prog. Surf. Sci.*, 1999, **61**, 127–198.

